EUROPEAN ORGANIZATION FOR NUCLEAR RESEARCH

CERN-AT-95-60

CERN AT/95-60 (MA)

Field, Forces and Mechanics of Superconducting Magnets

R. Perin

The chapter starts with a brief recall of the peculiar characteristics of superconducting magnets for accelerators, and of the evolution in performance of the main magnets of the most important projects. An outline of the concepts and methods used in the magnetic and mechanical design of the magnets is then presented together with some examples of applications and indications of the manufacturing accuracies necessary to achieve the required performance and field quality.

CERN ACCELERATOR SCHOOL, DESY, Hamburg
17-24 May 1995

Geneva, Switzerland
22 January 1996

FIELD, FORCES AND MECHANICS OF SUPERCONDUCTING MAGNETS

Romeo Perin
CERN, Geneva, Switzerland

Abstract
The chapter starts with a brief recall of the peculiar characteristics of superconducting magnets for accelerators, and of the evolution in performance of the main magnets of the most important projects. An outline of the concepts and methods used in the magnetic and mechanical design of the magnets is then presented together with some examples of applications and indications of the manufacturing accuracies necessary to achieve the required performance and field quality.

1. INTRODUCTION

Superconducting magnets have become essential components of hadron accelerator/colliders and of compact electron accelerators. For almost three decades high-energy physics has been the prime promoter of their development as the means to reach higher beam energy while minimising cost and space requirements.

There are some fundamental differences between superconducting magnets for accelerators and other superconducting magnets (e.g. large solenoids for particle detectors, toroidal coils for nuclear fusion machines, etc.) that make their design and construction a very special branch of the technology:

a) the need to use very high current densities to economically produce the required high bending/focusing fields;

b) the more complex and non-uniform repartition of electro-magnetic forces;

c) the extreme precision of the magnetic field distribution in small apertures;

d) the high degree of reproducibility and reliability.

Some of these characteristics make the task of building superconducting accelerator magnets singularly complex and difficult. In particular:

point a precludes cryogenic stabilization;

point b leads to elaborate mechanical structures;

point c demands an unprecedented dimensional precision in components and fabrication;

point d imposes fabrication methods adapted to large scale industrial production.

As in circular machines, the attainable beam energy is proportional to the machine radius and bending magnetic field, there is a great incentive to develop dipoles for higher and higher fields.

As a consequence the dipole magnets, which are the most important components of the accelerators from the cost point of view, also become the most critical technologically. In parallel, the focusing elements (quadrupoles) have to become stronger while being kept as short as possible.

The evolution in field and field gradient of superconducting main magnets for accelerators is recalled in Table 1.

Table 1
Design parameters of superconducting main magnets in accelerator/colliders

	Dipoles			Quadrupoles			Operation temperature
	Central field (T)	Coil aperture (mm)	Eff. unit length (m)	Field gradient (T/m)	Coil aperture (mm)	Eff. length (m)	(K)
TEVATRON	4.4	76.2	6.1	75.8	88.9	1.7	4.6
HERA	4.7	75	8.8	91.2	75	1.9/1.7	4.5
RHIC	3.5	80	9.5	71.8	80	1.1	4.6
UNK	5.0	80	5.7	96.1	80	3.0	4.6
SSC	6.6	50	15.2	206	40	5.2	4.35
LHC	8.4	56	14.2	223	56	3.1	1.9

Improvements in performance of superconductors, better insulation systems, force containment structures and refinements in manufacturing have permitted the field and gradient to be increased. A bold step is being made with the LHC using the superfluid helium technique, thus enhancing the performance of the traditional NbTi superconductor, and by the adoption of the two-in-one configuration leading to a considerable reduction of costs and size.

In modern proton or heavier particle high-energy accelerators the share of the magnet system in the cost of the facility is important. In the case of the LHC [1], which will be installed in the existing LEP tunnel, it is predominant (Fig. 1), the main dipoles and quadrupoles taking the largest share (Fig. 2). This chapter will mainly deal with these two types of magnets. The design and construction of the corrector magnets which are in general less demanding and can, therefore, be dimensioned with larger margins, follow the same pattern.

For a general introduction to superconducting magnets the book "Superconducting Magnets" by M.N. Wilson [2] is recommended. More specifically on accelerator magnets, an excellent treatment may be found in the lectures given by K.H. Mess and P. Schmüser at the CERN-DESY Accelerator School in 1988 [3]. An outline on high-field accelerator magnets can be found in "New Techniques for Future Accelerators III" [4].

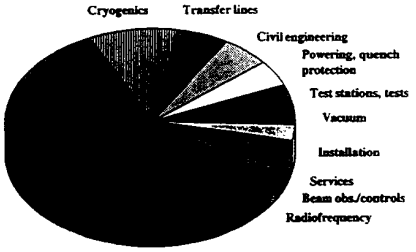

Fig. 1 Cost breakdown of LHC machine components

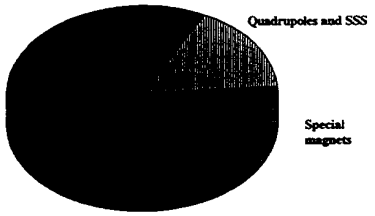

Fig. 2 Cost breakdown of LHC magnet system

2. CATEGORIES OF SUPERCONDUCTING MAGNETS FOR ACCELERATORS

Three different classes of magnets can be characterized with respect to the way in which the wanted field quality is achieved:

a) Magnets in which the field distribution is dominated by the coil configuration. The ISR and LEP quadrupoles, the Tevatron, HERA, RHIC, (SSC), LHC main dipoles and quadrupoles pertain to this class (Fig. 3).

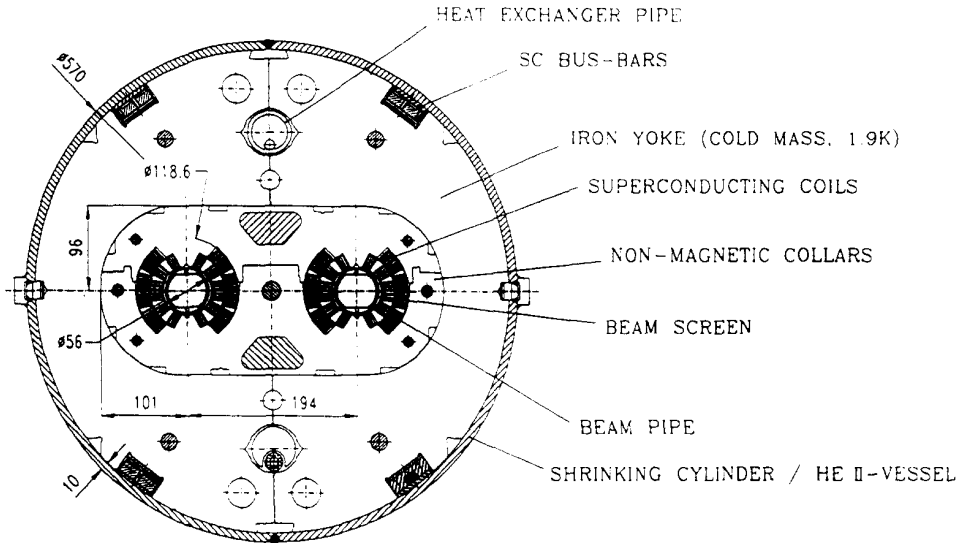

Fig. 3 Example of coil dominated magnet: the LHC dipole [1]

b) Iron dominated magnets, also called superferric, in which the iron (steel) pole shape determines the field pattern (examples of these are the HERA correctors, the RHIC sextupoles [5], etc.) (Fig. 4).

c) Magnets in which the field distribution results from the interplay of coils and yoke, both strongly contributing to produce the required field. Examples are some model magnets built at TAC and the configurations recently proposed by Texas A&M University and LBL of the "Block-Coil Dual Dipole" and of the "Pipe" magnet [6] (Fig. 5).

3. MAGNETIC DESIGN

3.1 General

In beam guiding magnets, the problem is essentially bidimensional because, apart from the localized regions of the ends, the field distribution has to be the same in all planes perpendicular to the beam axis. Type b) magnets are designed and built much in the same way as classical resistive magnets, the main difference being that they allow much higher current densities in the windings. So, for the magnetic design, use is made of the well developed finite differences and finite elements computer codes. For type c), the same methods apply, since the iron yoke plays an important role.

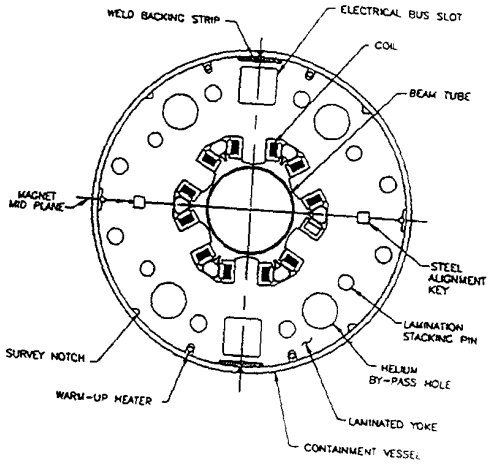

Fig. 4 Example of iron-dominated (super ferric) magnet: the RHIC arc sextupole

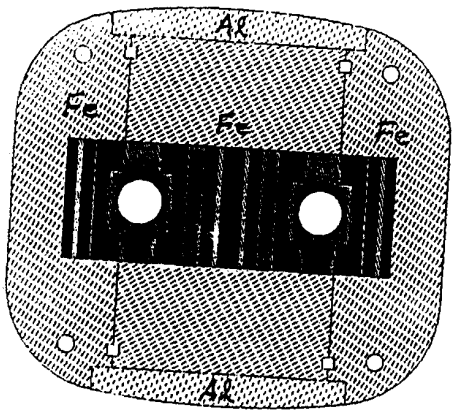

Fig. 5 Example of "mixed" magnet in which the field configuration is determined by conductor and iron: the Block-Coil Dual Dipole

In this lecture we treat only the magnetic design of type a) magnets as it is more typical of superconducting accelerator magnets. Generally the design starts with *analytical methods*, integrating the Biot-Savart law which describes the field (induction) induced by a current flowing through a (infinitely) thin wire:

$$\vec{B} = \frac{\mu_0}{4\pi} I \int_c \vec{d\ell} \times \frac{\vec{r}}{r^3} \qquad (1)$$

When the windings are not of simple geometry, they are subdivided into small regular parts whose contributions to the field can be computed analytically and summed by means of relatively simple computer programs.

In this first phase of the design, iron is in general assumed to have infinite magnetic permeability ($\mu = \infty$). Only in a second phase does one analyse the effects of the real iron characteristics, i.e. remanence, variable permeability and saturation. This is done by means of computer programs solving the partial differential equations by finite differences or finite elements numerical methods (e.g. POISSON, MARE/MAGNET, TOSCA [7–9], etc.).

3.2 Ideal current distributions generating typical field configurations for accelerators (dipole, quadrupole, sextupole, etc.) and practical approximations

A line current distributed on a circular cylindrical surface as a function of the azimuthal angle ϑ according to:

$$I(\vartheta) = I_o \cos(n\vartheta) \qquad (2)$$

generates a pure 2 n-pole field inside the circular aperture (Fig. 6).

Pure 2 n-pole fields are also obtained by means of uniformly distributed currents flowing in conductors of particular shape. The simplest of these ideal shapes, producing a dipole field, is formed by the intersection of two cylinders with their centres spaced apart and carrying oppositely directed currents with uniform density.

More generally pure multipole fields can be obtained in the aperture formed by the overlap region of equal conductors of elliptical cross-section suitably spaced and having uniform current

densities of convenient sign. In fact, it has been shown by Beth [10] that the internal field of an elliptical conductor with semi-axis a and b in the x and y directions respectively and uniform current density J is:

$$\vec{B} = \vec{B}_x + \vec{B}_y \qquad B_x = -\frac{\mu o\, J}{a+b}\, a\, y \qquad B_y = \frac{\mu o}{a+b}\, b\, x \tag{3}$$

Examples are shown in Fig. 6. If two ellipses are aligned along their major axis, a pure dipole is produced, if they overlap at right angles the field in the overlap is a pure quadrupole.

The practical approximations to the above ideal configuration are shown in Fig. 7 for the dipoles and Fig. 8 for the quadrupoles.

3.3 Design of the coil configuration using an analytic/numerical approach

The field distribution produced by the practical approximations to the ideal coil cross-sections can be computed by means of analytic programs, which can take into account the presence of a circular steel screen, considered as an equipotential surface ($\mu = \infty$), around the windings.

The treatment presented here follows the note of Ref. [11]. The field produced by a current flowing through the surface S (Fig. 9) perpendicularly to the x, y plane is given by the Biot-Savart law in two dimensions:

$$\vec{B} = \frac{\mu o}{2\pi} \iint \frac{\vec{J}(x, y) \times \vec{r}}{r^2}\, ds \tag{4}$$

where the current density $\vec{J}$ is flowing perpendicularly to the plane of $\vec{B}$ in infinitely long conductors.

Field generated by the current $I = \int_S J(x, y)\, ds$:

$$|B| = \frac{\mu o}{2\pi} \iint \frac{J(x, y)}{r}\, ds = \frac{\mu o}{2\pi} \iint \frac{J(x, y)}{\sqrt{(x-x_c)^2 + (y-y_c)^2}}\, ds \tag{5}$$

$$B_x = |B| \sin\alpha = -\frac{\mu o}{2\pi} \iint \frac{J(x, y)}{(x-x_c)^2 + (y-y_c)^2} .(y-y_c)\, ds \tag{6}$$

$$B_y = |B| \cos\alpha = \frac{\mu o}{2\pi} \iint \frac{J(x, y)}{(x-x_c)^2 + (y-y_c)^2} .(x-x_c)\, ds \tag{7}$$

The treatment is particularly simple using the analytic function* F

$$\vec{F} = B_y + iB_x = \frac{\mu o}{2\pi} \iint \frac{J(x, y)\,(x-x_c)}{(x-x_c)^2 + (y-y_c)^2} ds + i\,(-\frac{\mu o}{2\pi}) \iint \frac{J(x, y)\,(y-y_c)}{(x-x_c)^2 + (y-y_c)^2}\, ds \tag{8}$$

$$= \frac{\mu o}{2\pi} \iint \frac{J(x, y)}{z - z_c}\, ds \qquad \text{valid for all } z \neq z_c$$

If a circular steel screen with $\mu = \infty$ is present around the coil, its contribution can be calculated with the image current method:

---

* Note: The magnetic field (induction) $\vec{B} = B_x + iB_y$ is not an analytic function as it does not satisfy the Cauchy-Riemann conditions.

Cos nϑ

Intersecting ellipses

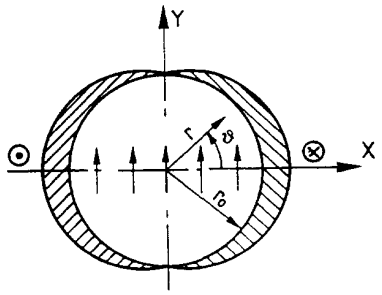

Dipole

$I = I_o \cos \vartheta$

J uniform in the hatched areas

$B_\vartheta = \frac{\mu o\ I_o}{2\ r_o} \cos \vartheta$ $\qquad B_x = o$ $\qquad B_x = o$

$B_\vartheta = \frac{\mu o\ I_o}{2\ r_o} \sin \vartheta$ $\qquad B_y = \frac{\mu o\ I_o}{2\ r_o}$ $\qquad B_y = \mu o\ J\ \frac{sb}{a + b}$

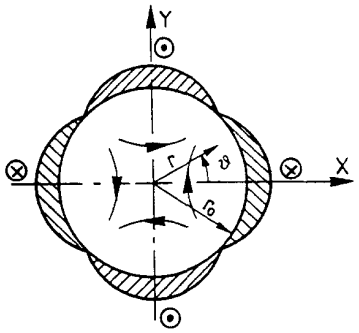

Quadrupole

$I = I_o \cos 2\ \vartheta$

J uniform in the hatched areas

$B_x = \frac{\mu o\ I_o}{2\ r_o^2}\ y$ $\qquad B_x = \mu o\ J\ \frac{a-b}{a+b}\ y$

$B_y = \frac{\mu o\ I_o}{2\ r_o^2}\ x$ $\qquad B_y = \mu o\ J\ \frac{a-b}{a+b}\ x$

$G = \frac{\mu o\ I_o}{2\ r_o^2}$ $\qquad G = \mu o\ J\ \frac{a-b}{a+b}$

Fig. 6 Ideal current distributions producing pure dipole and quadrupole fields

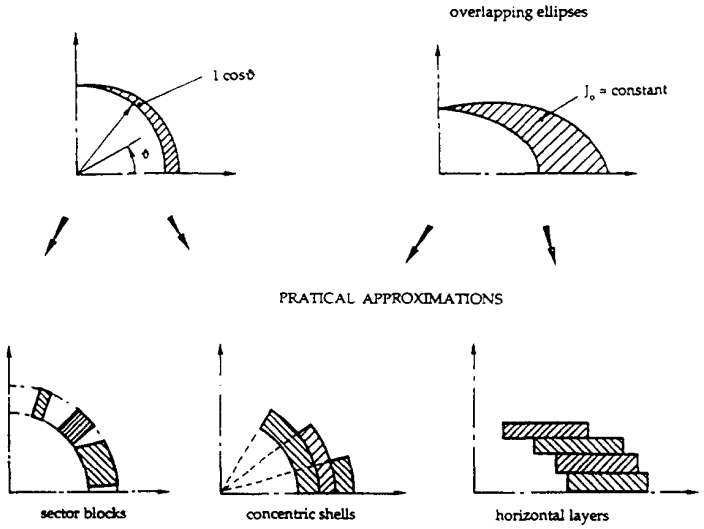

Fig. 7 Dipole ideal configurations and practical approximations

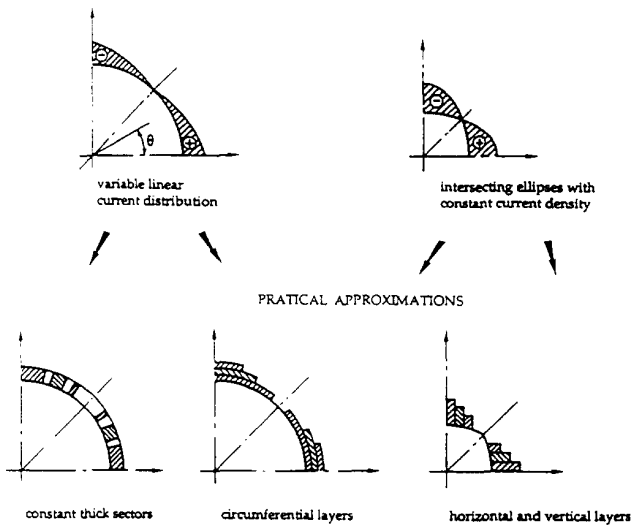

Fig. 8 Quadrupole ideal configurations and practical approximations

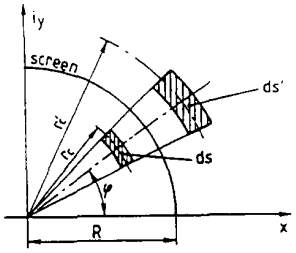

Fig. 9

J directed upwards

In the complex plane $z = x + iy$,

$z = x + iy$ coordinate of the point where the field B is calculated

$z_c = x_c + iy_c$ coordinate of conductor element ds

$$r'_c = \frac{R^2}{r_c} \qquad J' = J\left(\frac{R}{r'_c}\right)^4 \qquad ds' = \frac{R^4}{r_c^4}\,ds \qquad z'_c = \frac{R^2}{r_c}\,e^{i\phi}$$

$$F = B_y + iB_x = \frac{\mu o}{2\pi}\iint \frac{J}{z - z_c}\,ds + \frac{\mu o}{2\pi}\iint \frac{J}{z - \frac{R^2}{z_c^*}}\,ds \qquad (9)$$

$$\frac{1}{z-z_c} = -\frac{1}{z_c\left(1-\frac{z}{z_c}\right)} = -\frac{1}{z_c}\sum_{o}^{\infty} k\left(\frac{z}{z_c}\right)^k = -\frac{1}{z_c}\sum_{1}^{\infty} n\left(\frac{z}{z_c}\right)^{n-1} = -\sum_{1}^{\infty}\frac{z^{n-1}}{z_c^{\,n}}$$

$$\frac{1}{z-\frac{R^2}{z_c^*}} = -\frac{1}{\frac{R^2}{z_c^*}\left(1-\frac{z\,z_c^*}{R^2}\right)} = -\frac{z_c^*}{R^2}\sum_{1}^{\infty} n\left(\frac{z\,z_c^*}{R^2}\right)^{n-1} = -\sum_{1}^{\infty} n\, z^{n-1}\,\frac{z_c^{*n}}{R^{2n}}$$

$$\boxed{F = -\sum_{1}^{\infty}(c_n + f_n)\, z^{n-1}} \qquad (10)$$

with

$c_n = \frac{\mu_o}{2\pi}\iint J\, z_c^{-n}\, ds$	Direct contribution of the coil to the n component	(11)
$f_n = \frac{\mu_o}{2\pi}\iint J\,\frac{z^{*n}_c}{R^{2n}}\, ds$	Contribution of the iron screen to the n component.	(12)

For circular sector windings defined by the radii r_1 and r_2 and the angles ϕ_1 and ϕ_2

$$z_c = r_c\, e^{i\phi} \qquad c_n = \frac{\mu_o}{2\pi}\int_{r_1}^{r_2}\int_{\phi_1}^{\phi_2} J\, r^{-n}\, e^{-in\phi}\, r\,dr\,d\phi = \frac{\mu_o}{2\pi}\int_{r_1}^{r_2}\int_{\phi_1}^{\phi_2} J\, r^{1-n}\, e^{-in\phi}\, dr\,d\phi \qquad (13)$$

If J is constant in the element $r_2 - r_1$, $\phi_2 - \phi_1$

$$c_n = \frac{\mu_o}{2\pi} J\left[\frac{r_c^{2-n}}{2-n}\right]_{r_1}^{r_2}\left[e^{-in\phi}\right]_{\phi_1}^{\phi_2}\frac{1}{-in} = i\,\frac{\mu_o}{2\pi}\,\frac{J}{(2-n)n}\left(r_2^{2-n}-r_1^{2-n}\right)\left(e^{-in\phi_2}-e^{-in\phi_1}\right) \qquad (14)$$

For n = 2,

$$c_2 = i\frac{\mu_o}{4\pi}\, J\, \ell n\,\frac{r_2}{r_1}\left(e^{-in\phi_2} - e^{-in\phi_1}\right) \qquad (15)$$

For the case of symmetrical windings with respect to the horizontal median plane (Fig. 10): $\phi_1 = -\phi$ $\phi_2 = \phi$

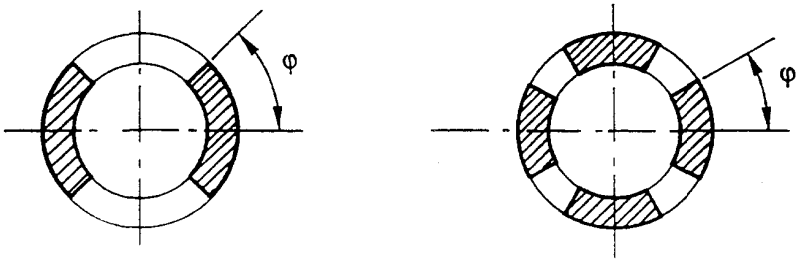

Fig. 10 Symmetries: dipole and quadrupole

$$c_n = i \frac{\mu o}{2\pi} \frac{J}{(2-n)n} (r_2^{2-n} - r_1^{2-n}) (e^{-in\phi} - e^{+in\phi})$$

For $n \neq 2$,

$$c_n = \frac{\mu o}{\pi} \frac{J}{n(2-n)} (r_2^{2-n} - r_1^{2-n}) \sin n \phi \tag{16}$$

$$f_n = \frac{\mu o}{2\pi} \frac{1}{r^{2n}} \int_{r_1}^{r_2} \int_{\phi_1}^{\phi_2} J r_c^{n+1} e^{-in\phi} \, dr d\phi = \frac{\mu o}{\pi} \frac{J}{R^{2n}} \frac{}{n(n+2)} (r_2^{n+2} - r_1^{n+2}) \sin n \phi \tag{17}$$

For $n = 2$,

$$c_2 = \frac{\mu o}{2\pi} \int_{r_1}^{r_2} \frac{1}{r} dr \int_{-\phi}^{+\phi} e^{-i\,2\phi} \, d\phi = \frac{\mu o J}{2\pi} \ell n \frac{r_2}{r_1} \sin 2 \phi \tag{18}$$

$$f_2 = \frac{\mu o}{\pi} J \frac{r_2^4 - r_1^4}{4R^4} \sin 2 \phi \tag{19}$$

For a <u>dipole</u>, it is convenient to add the sector $\pi + \phi$, $\pi - \phi$.

For $n = 1, 3, 5, 7, 9 \ldots$,

$$\boxed{c_{n_d} = \frac{2\mu o}{\pi} \frac{J (r_2^{2-n} - r_1^{2-n})}{n(2-n)} \sin n \phi} \tag{20}$$

$$f_{n_d} = \frac{2\mu o}{\pi} \frac{J}{R^{2n}} \frac{(r_2^{n+2} - r_1^{n+2})}{n(n+2)} \sin n \phi \tag{21}$$

For a <u>quadrupole</u>, it is convenient to add the sectors $\pi + \phi$, $\pi - \phi$ and $\frac{\pi}{2} + \phi$, $\frac{\pi}{2} - \phi$ and $\frac{3}{2}\pi + \phi$, $\frac{3}{2}\pi - \phi$:

For $n \neq 2$,

$$c_{n_q} = \frac{4\mu o}{\pi} \frac{J (r_2^{2-n} - r_1^{2-n})}{n(2-n)} \sin n \phi \tag{22}$$

For $n = 2$,

$$c_{2_q} = \frac{2\mu o}{\pi} J \ell n \frac{r_2}{r_1} \sin 2 \phi \tag{23}$$

For $n = 2, 6, 10, 14, 18 \ldots$,

$$f_{n_q} = \frac{4\mu o}{\pi} \frac{J}{R^{2n}} \frac{r_2^{n+2} - r_1^{n+2}}{n(n+2)} \sin n \phi \tag{24}$$

Elimination of multipoles

Unwanted higher-order multipoles can be eliminated by conveniently choosing the angles, the thickness and the current density in the different parts of the windings. For example, for coils composed of m sector blocks with the same inner and outer radii (r_1, r_2) and uniform current density, the condition to be satisfied is

$$\sum_{1}^{m}{}_{K} \; J \sin n \, \phi_k = 0 \qquad (25)$$

For a dipole, to eliminate the first higher multipole, the 6-pole, the condition J sin 3 f = 0 has to be satisfied, which leads to f = 60°. Therefore one block of conductors extending from the median plane to the 60° angle is sufficient.

If the coils are composed of two sector blocks of conductors (per quadrant), the first three higher multipoles, 6-pole, 10-pole, 14-pole, can be eliminated.

For a quadrupole, a single block sector winding (per octant) is sufficient to suppress the first higher-order multipole, the 12-pole. For this, the block has to cover the sector from the median plane to the angle $\phi = 30°$. If one wants to suppress the 12-pole, the 20-pole and the 28-pole, a two-block winding is necessary with angles $\phi_1 = 21.59°$, $\phi_2 = 26.075°$, $\phi_3 = 33.635°$. A three-block winding also allows the 36- and the 44-pole to be eliminated: for this the angles are $\phi_1 = 16.657°$, $\phi_2 = 18.548°$, $\phi_3 = 26.564°$, $\phi_4 = 31.682°$, $\phi_5 = 35.915°$.

If the coils are composed of two or more shells, one can adjust the different current densities, angles and subdivision in the conductor blocks in each layer in order to reduce the unwanted multipoles to acceptable values.

Real geometry

In general, the real geometry of the current carrying area does *not* consist of *perfect circular sectors*, because the conductors are rectangular or of a keystone shape and are surrounded and separated by insulation. To treat this, one subdivides each winding block or shell into a number of small circular sectors of uniform current density. The field produced by each element is separately computed and then added up with the field produced by all other elements. This is normally done by means of relatively simple computer programs, such as part of ROXIE [12].

Real iron screen (variable μ)

At this point, one applies one of the existing two-dimensional computer programs, such as MARE/MAGNET, POISSON, etc., in order to optimize yoke thickness, yoke-coil distance, and yoke shape.

In this way the disposition of the conductor around the aperture and in general the magnet cross-section are determined. Figures 3 and 11 show some examples of coil configurations and magnet cross-sections determined by the above method.

3.4 End shaping

In superconducting magnets the coil end is usually the most problematic part in terms of design, winding and mechanical support. The conductors are bent in a saddle fashion around the cylindrical aperture and this is particularly demanding in dipole magnets where the outer turns have to be bent through 180°.

The coil-end shape is optimized, taking into account various requirements:

- ease of fabrication: maximization of the smallest radius of curvature of the conductor in each block;
- mechanical stability;

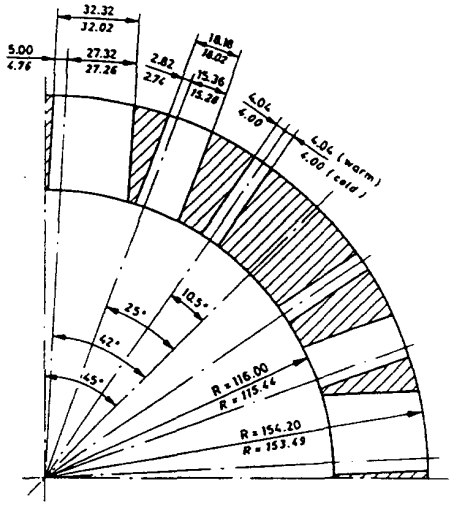

Fig. 11 ISR quadrupoles: cross-section of coil with warm and cold dimensions [13]

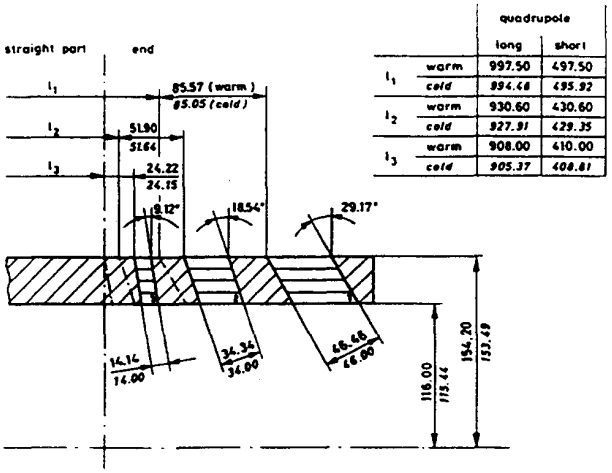

		quadrupole long	quadrupole short
l_1	warm	997.50	497.50
	cold	994.48	495.92
l_2	warm	930.60	430.60
	cold	927.91	429.35
l_3	warm	908.00	410.00
	cold	905.37	408.81

Fig. 12 ISR quadrupoles: coil-end cut along the 45° plane with warm and cold dimensions [13]

- limitation of maximum field in the coils to a value below the max. field in the straight part in order not to limit the magnet performance;
- field quality, i.e. minimum multipole content integrated over the coil end;
- minimization of the end length to limit the loss of magnetic length.

In general, at the ends the coil is spread out in conductor blocks separated by spacers whose number, shape and dimensions are determined by the above requirements. Concerning the shape of the conductor bends, two types are mainly used: conductors upright with their wide face perpendicular to the aperture cylindrical surface, e.g. the HERA dipole coils, and the quasi-isoperimetric form approximating the shape that a thin tape would naturally take (e.g. ISR quadrupoles, LHC magnets). The first configuration entails considerable deformation of the cable, but has the advantage of "filling" the same cylindrical space as in the straight part of the magnet. The other configuration is more adapted to large conductors as the resulting deformation is smaller, but the conductors take an inclination with respect to the magnet axis. Consequently some filler material is needed to restore the cylindrical surfaces through which the electro-magnetic forces are transferred to the supporting structure. Several variants of these configurations have been used, examples are shown in Figs. 12–15.

a) spaces to be filled to restore the outer cylinder of each coil layer

b) spaces to be filled to restore the inner cylinder of each coil layer

Fig. 13 Cut through two quasi-isoperimetric ends (LHC dipole models)

The calculations are carried out with the aid of computer programs. These may be analytical and based on the formulae outlined in section 3.3, taking advantage of the fact that the field integrated from $-\infty$ to $+\infty$ or from the magnet centre to ∞ satisfies Laplace's equation in two dimensions, such as the programs ENDEF [14] or ROXIE. Other programs integrate the Biot-Savart law point by point [15]. With these programs however, the iron is considered as an equipotential boundary ($\mu = \infty$). To take into account the effects of iron saturation more complex finite-element programs are used (e.g. TOSCA) [16].

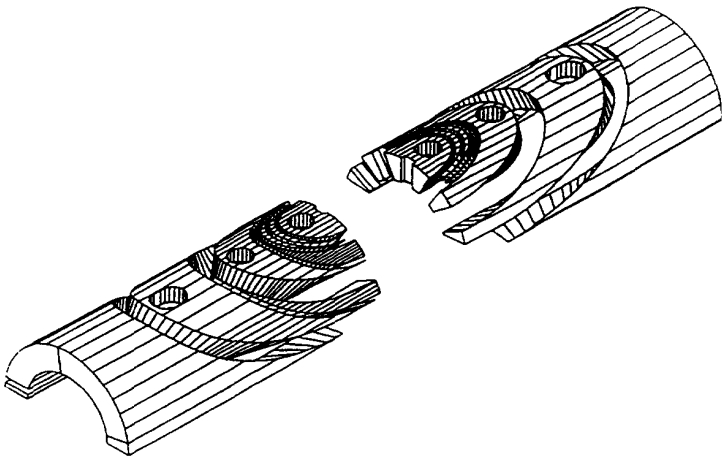

Fig. 14 End spacers for the LHC dipole coil inner shell

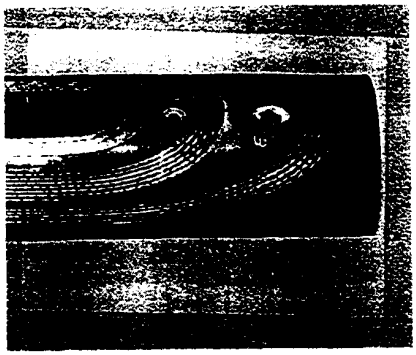

Fig. 15 Coil end (LHC dipole model, inner shell)

3.5 Other points studied in the magnetic design

Effects of remanent field { from the conductor (persistent currents). / from the yoke (or screen).

Stored energy, stray field.

Tolerances on geometry.

Electro-magnetic forces, etc.

4. FIELD QUALITY

Field quality is, of course of great importance to the accelerator designer, as it directly affects beam optics and stability of the beam(s).

4.1 Definition of multipole field components

The field in accelerator magnets can usually be treated as two-dimensional since the beam integrates through the field. It can then be expressed as a power series:

$$B_y + iB_x = B_1 \sum_{1}^{\infty} {}_n (b_n + ia_n)\,(z/R_r)^{n-1}$$

where B_1 = magnitude of dipole field in the y (vertical) direction;
b_n = normal multipole coefficient;
a_n = skew multipole coefficient
z = $x + iy$;
R_r = reference radius.

n = 1 dipole
n = 2 quadrupole
n = 3 sextupole, etc.

One has to be careful when comparing figures, because the coefficients a_n and b_n are dimensionally dependent. So they must be defined at a given reference radius.

Caution

When consulting literature, attention has to be paid to the fact that in the USA a slightly different nomenclature is used:

$$B_y + iB_x = B_o \sum_0^\infty {}_n (b_n + ia_n) (z/R_r)^n$$

and then n = 0 dipole,
n = 1 quadrupole,
n = 2 sextupole, etc.

4.2 Sources of field errors

Field errors have different origins: conductor placement errors, iron saturation, coil deformations under e.m. forces, persistent and eddy currents.

a) Conductor placement errors

The field errors originating from misalignment of conductors or complete coils can be computed analytically at the design stage from the known possible or imposed manufacturing tolerances. Sensitivity matrices can be computed for displacement of single conductors or conductor blocks, as for example the matrix of Fig. [16] for the LHC dipole, which has a coil aperture diameter of 56 mm [17]. Some examples are given for this magnet in terms of the most sensitive multipole components a_n, b_n defined at the reference radius R_r = 10 mm:

- a 0.1-mm increase of the coil azimuthal size (which incidentally would correspond to a compression of about 30 MPa) while current and coil thickness remain unchanged, produces a sextupole and a decapole

$$b_3 = 1.2 \times 10^{-4}, \qquad b_5 = 0.03 \times 10^{-4}$$

- a 0.01-mm inner radius difference between lower and upper poles of the same aperture produces a skew quadrupole

$$a_2 = 0.44 \times 10^{-4}$$

- a 0.1-mm vertical off-centering of the coils with respect to the yoke produces a skew quadrupole

$a_2 = 0.15 \times 10^{-4}$ at 0.58 T (injec. field), and 0.09×10^{-4} at 8.4 T (nominal field)

- a 1-mm difference in length between lower and upper coil of the same aperture in a 14 m long LHC dipole ($\Delta L/L = 7 \times 10^{-5}$) is equivalent to an "integrated two-dimensional" skew quadrupole

$$a_2 = 0.06 \times 10^{-4}$$

Fluctuations of bending power from magnet to magnet may be also originated:

- a 0.1-mm azimuthal elongation of the coils, with unchanged current and coil thickness, produces a dipole field variation

$$\frac{\Delta B}{B} = - 1.4 \times 10^{-3}$$

– a 0.1-mm increase of coil inner radius, with unchanged current and coil thickness, produces

$$\frac{\Delta B}{B} = - 1.5 \times 10^{-3}$$

– a 0.1-mm increase of yoke aperture (coil-yoke distance) produces

$$\frac{\Delta B}{B} = - 1.5 \times 10^{-3}$$

Error matrix for radial displacements of 1 mm of the winding blocks in 1E-4

		Quadrant 1					Quadrant 2					Quadrant 3					Quadrant 4				
Error type	Multipole order	Block 1.1	1.2	1.3	1.4	1.5	Block 2.1	2.2	2.3	2.4	2.5	Block 3.1	3.2	3.3	3.4	3.5	Block 4.1	4.2	4.3	4.4	4.5
b_n	1	-7.89	-8.45	-9.18	-9.20	-3.36	-7.89	-8.45	-9.18	-9.20	-3.36	-7.89	-8.45	-9.18	-9.20	-3.36	-7.89	-8.45	-9.18	-9.20	-3.36
a_n	1	1.48	6.87	1.42	6.28	6.64	-1.48	-6.87	-1.42	-6.28	-6.64	1.48	6.87	1.42	6.28	6.64	-1.48	-6.87	-1.42	-6.28	-6.64
b_n	2	3.68	1.08	5.70	2.60	-2.88	-3.68	-1.08	-5.70	-2.60	2.88	-3.68	-1.08	-5.70	-2.60	2.88	3.68	1.08	5.70	2.60	-2.88
a_n	2	-1.44	-5.18	-1.85	-6.67	-3.88	-1.44	-5.18	-1.85	-6.67	-3.88	1.44	5.18	1.85	6.67	3.88	1.44	5.18	1.85	6.67	3.88
b_n	3	-1.02	0.73	-2.33	0.71	2.09	-1.02	0.73	-2.33	0.71	2.09	-1.02	0.73	-2.33	0.71	2.09	-1.02	0.73	-2.33	0.71	2.09
a_n	3	0.64	1.40	1.20	3.02	-0.37	-0.64	-1.40	-1.20	-3.02	0.37	0.64	1.40	1.20	3.02	-0.37	-0.64	-1.40	-1.20	-3.02	0.37
b_n	4	0.23	-0.36	0.81	-0.87	-0.23	-0.23	0.36	-0.81	0.87	0.23	-0.23	0.36	-0.81	0.87	0.23	0.23	-0.36	0.81	-0.87	-0.23
a_n	4	-0.21	-0.16	-0.60	-0.80	0.79	-0.21	-0.16	-0.60	-0.80	0.79	0.21	0.16	0.60	0.80	-0.79	0.21	0.16	0.60	0.80	-0.79
b_n	5	-0.04	0.09	-0.25	0.42	-0.22	-0.04	0.09	-0.25	0.42	-0.22	-0.04	0.09	-0.25	0.42	-0.22	-0.04	0.09	-0.25	0.42	-0.22
a_n	5	0.06	-0.02	0.26	0.06	-0.20	-0.06	0.02	-0.26	-0.06	0.20	0.06	-0.02	0.26	0.06	-0.20	-0.06	0.02	-0.26	-0.06	0.20
b_n	6	0.01	-0.01	0.07	-0.13	0.10	-0.01	0.01	-0.07	0.13	-0.10	-0.01	0.01	-0.07	0.13	-0.10	0.01	-0.01	0.07	-0.13	0.10
a_n	6	-0.02	0.02	-0.10	0.06	-0.04	-0.02	0.02	-0.10	0.06	-0.04	0.02	-0.02	0.10	-0.06	0.04	0.02	-0.02	0.10	-0.06	0.04
b_n	7	0.00	0.00	-0.02	0.02	0.00	0.00	0.00	-0.02	0.02	0.00	0.00	0.00	-0.02	0.02	0.00	0.00	0.00	-0.02	0.02	0.00
a_n	7	0.00	0.00	0.04	-0.04	0.04	0.00	0.00	-0.04	0.04	-0.04	0.00	0.00	0.04	-0.04	0.04	0.00	0.00	-0.04	0.04	-0.04
b_n	8	0.00	0.00	0.00	0.00	-0.01	0.00	0.00	0.00	0.00	0.01	0.00	0.00	0.00	0.00	0.01	0.00	0.00	0.00	0.00	-0.01
a_n	8	0.00	0.00	-0.01	0.01	-0.01	0.00	0.00	-0.01	0.01	-0.01	0.00	0.00	0.01	-0.01	0.01	0.00	0.00	0.01	-0.01	0.01
b_n	9	0.00	0.00	0.00	0.00	0.00	0.00	0.00	0.00	0.00	0.00	0.00	0.00	0.00	0.00	0.00	0.00	0.00	0.00	0.00	0.00
a_n	9	0.00	0.00	0.00	0.00	0.00	0.00	0.00	0.00	0.00	0.00	0.00	0.00	0.00	0.00	0.00	0.00	0.00	0.00	0.00	0.00

Error matrix for tangential displacements of 1mm of the winding blocks in 1E-4

		Quadrant 1					Quadrant 2					Quadrant 3					Quadrant 4				
Error type	Multipole order	Block 1.1	1.2	1.3	1.4	1.5	Block 2.1	2.2	2.3	2.4	2.5	Block 3.1	3.2	3.3	3.4	3.5	Block 4.1	4.2	4.3	4.4	4.5
b_n	1	-2.76	-12.30	-2.03	-8.30	-8.66	2.49	12.01	1.70	7.97	8.54	-2.76	-12.30	-2.03	-8.30	-8.66	2.49	12.01	1.70	7.97	8.54
a_n	1	-13.93	-14.84	-11.86	-11.79	-4.22	-13.98	-15.07	-11.91	-12.02	-4.46	-13.93	-14.84	-11.86	-11.79	-4.22	-13.98	-15.07	-11.91	-12.02	-4.46
b_n	2	1.78	6.10	2.07	6.94	3.91	1.61	6.05	1.74	6.79	4.07	-1.78	-6.10	-2.07	-6.94	-3.91	-1.61	-6.05	-1.74	-6.79	-4.07
a_n	2	4.29	1.15	5.82	2.48	-3.07	-4.35	-1.38	-5.93	-2.86	2.85	-4.29	-1.15	-5.82	-2.48	3.07	4.35	1.38	5.93	2.86	-2.85
b_n	3	-0.71	-1.45	-1.30	-2.99	0.46	0.65	1.49	1.10	3.05	-0.28	-0.71	-1.45	-1.30	-2.99	0.46	0.65	1.49	1.10	3.05	-0.28
a_n	3	-1.06	0.81	-2.28	0.83	2.08	-1.10	0.72	-2.38	0.58	2.11	-1.06	0.81	-2.28	0.83	2.08	-1.10	0.72	-2.38	0.58	2.11
b_n	4	0.23	0.15	0.64	0.74	-0.80	0.21	0.17	0.55	0.84	-0.78	-0.23	-0.15	-0.64	-0.74	0.80	-0.21	-0.17	-0.55	-0.84	0.78
a_n	4	0.23	-0.37	0.77	-0.91	-0.19	-0.24	0.36	-0.84	0.82	0.28	-0.23	0.37	-0.77	0.91	0.19	0.24	-0.36	0.84	-0.82	-0.28
b_n	5	-0.06	0.03	-0.28	-0.03	0.19	0.06	-0.02	0.24	0.09	-0.22	-0.06	0.03	-0.28	-0.03	0.19	0.06	-0.02	0.24	0.09	-0.22
a_n	5	-0.04	0.09	-0.23	0.42	-0.24	-0.05	0.09	-0.27	0.41	-0.21	-0.04	0.09	-0.23	0.42	-0.24	-0.05	0.09	-0.27	0.41	-0.21
b_n	6	0.02	-0.02	0.11	-0.07	0.05	0.02	-0.01	0.10	-0.05	0.03	-0.02	0.02	-0.11	0.07	-0.05	-0.02	0.01	-0.10	0.05	-0.03
a_n	6	0.01	-0.01	0.08	-0.12	0.10	-0.01	0.01	-0.08	0.13	-0.10	-0.01	0.01	-0.08	0.12	-0.10	0.01	-0.01	0.08	-0.13	0.10
b_n	7	0.00	0.00	-0.04	0.04	-0.04	0.00	0.00	0.04	-0.04	0.04	0.00	0.00	-0.04	0.04	-0.04	0.00	0.00	0.04	-0.04	0.04
a_n	7	0.00	0.00	-0.01	0.02	0.00	0.00	0.00	-0.02	0.03	-0.01	0.00	0.00	-0.01	0.02	0.00	0.00	0.00	-0.02	0.03	-0.01
b_n	8	0.00	0.00	0.01	-0.01	0.01	0.00	0.00	0.01	-0.02	0.01	0.00	0.00	-0.01	0.01	-0.01	0.00	0.00	-0.01	0.02	-0.01
a_n	8	0.00	0.00	0.00	0.00	-0.01	0.00	0.00	-0.01	0.00	0.01	0.00	0.00	0.00	0.00	0.01	0.00	0.00	0.01	0.00	-0.01
b_n	9	0.00	0.00	0.00	0.00	0.00	0.00	0.00	0.00	0.00	0.00	0.00	0.00	0.00	0.00	0.00	0.00	0.00	0.00	0.00	0.00
a_n	9	0.00	0.00	0.00	0.00	0.00	0.00	0.00	0.00	0.00	0.00	0.00	0.00	0.00	0.00	0.00	0.00	0.00	0.00	0.00	0.00

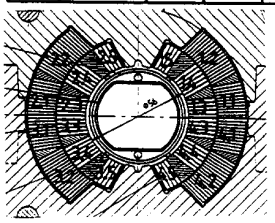

Fig. 16 Sensitivity matrix for radial and azimuthal displacements of conductor blocks in LHC dipole

From these examples one may understand how difficult it is to obtain in superconducting magnets a field quality comparable to that of classical lower field magnets, where the field distribution is determined by the iron-pole profiles which can easily be produced with a hundredth-millimetre precision. In superconducting magnets the coil geometry is the result of assembling stacks of conductors, typically 15 to 20, which are produced with stringent, but not infinitely small, tolerances (in cables the best that can be achieved nowadays is of the order of $\pm$ 0.0025 mm on the thickness) and insulated by wrapping them with tapes which can be industrially produced with a few micrometers tolerance on their thickness.

b) Iron saturation

The field errors originating from the remanence and the variable permeability vary with excitation and depend strongly on the coil-yoke distance. For warm iron magnets (e.g. Tevatron dipoles) these errors can be neglected in practice. For cold iron magnets they have to be carefully evaluated, are in general systematic and affect mainly the first higher multipoles (6-pole and 10-pole in dipoles) and can be compensated either by correction windings in the aperture (e.g. HERA) or by small corrector magnets placed at the magnet ends (e.g. LHC).

c) Coil deformation under the e.m. forces

These errors vary with excitation and can be easily computed after the mechanical analysis of the structure and the determination of the deformed coil configurations, using analytical or other computer programs.

d) Persistent currents in the superconductors

The persistent current errors are a particularity of superconducting magnets. They are due to currents induced in the superconducting filaments by field variations and, contrary to normal conductors where resistance rapidly reduces and after a while eliminates eddy currents, circulate indefinitely as long as the superconductor is kept below its critical temperature. Persistent current errors affect all field multipole components allowed by the symmetry configuration of the magnet, including the fundamental one. Their importance decreases with excitation, but they are particularly disturbing at low field level and especially at injection. They depend on the previous powering of the magnet and vary with time and, therefore, require a careful study of the magnet excitation cycle. Persistent currents are proportional to the effective diameter of the superconducting filaments, so accelerator magnets use filaments as thin as possible, compatibly with economy and quality of production.

This subject is extensively treated in the chapter by A. Devred and in Refs. [3, 18, 19].

e) Eddy currents

Eddy currents occur during field sweep in multistrand conductors both inside the strands, mainly due to coupling between filaments, and between the strands. They distort the magnetic field, and their effects depend on the geometrical and electrical characteristics of strands and cables (matrix and inter-strand resistance, cable aspect ratio, distribution of superconducting filaments, etc.) and, of course, on the field ramp rate.

This subject is also treated in a lecture by A. Devred and in Refs. [20–22].

f) Torsion

In long and slim objects such as superconducting magnets, twist around the longitudinal axis is difficult to prevent and can produce non-negligible field orientation errors. In general a tolerance of about 1 mrad is required in dipole magnets, and, although the beam integrates along its path, local twists should not exceed this value by more than a factor two or three. Excessive twist can be prevented by locking the magnet active part to a structural component of high torsional rigidity, generally a closed cylinder of large diameter, such as the helium vessel, which in many cases is also part of the force containment structure.

4.3 Examples

At the design stage of accelerators, forecasts of field quality can be obtained by applying the considerations of section 4.2. These can be corroborated by existing statistical results, at

present from the Tevatron (744 dipoles), from HERA (~ 500 dipoles) and recently from RHIC (~ 100 dipoles measured), and from LHC models and prototypes.

As an example, Table 2 presents the expected error field components in the LHC dipole at injection and nominal operation field. Table 3 shows an estimate of the eddy current errors for given interstrand contact resistance and field ramp rate: note that, *at a given ramp rate, eddy currents produce the same errors at any field level*, so that the relative field errors are highest at injection.

An example of twist in 10-m long magnets is shown in Fig. 17, plotting the field orientation in the two apertures of three LHC dipole prototypes of the first generation. Noticeable is the remarkably good parallelism of the field in the two apertures at all longitudinal positions.

5. FORCES AND MECHANICS

5.1 Some facts

– Electromagnetic forces (e.m.) are in first approximation proportional to B^2

$$\vec{F} = \vec{I} \times \vec{B} = \sim B^2$$

and are extremely high in high-field magnets: e.g. see in Fig. 18 the transverse forces in the LHC dipole.

Table 2
Expected multipole performance, at injection and at 8.40 T
(In units of 10^{-4} relative field error at 10 mm)

	At injection, 0.58 T				At nominal operation, 8.40 T			
	Mean		Random		Mean		Random	
n	norm. b_n	skew a_n	norm. $\sigma[b_n]$	skew $\sigma[a_n]$	norm. b_n	skew a_n	norm. $\sigma[b_n]$	skew $\sigma[a_n]$
2	±0.5	±0.3	0.4	1.0	1.0±0.5	±0.3	0.4	1.0
3	-3.6±0.3*	±0.3	0.5	0.15	0.5±0.3*	±0.3	0.6	0.15
4	±0.2	±0.2	0.1	0.1	±0.2	±o.2	0.1	0.1
5	0.18±0.05*	±0.05	0.08	0.04	0.06±0.05*	±0.05	0.05	0.04
6	-0.004	0.0	0.02	0.01	-0.005	0.0	0.006	0.01
7	-0.026	0.0	0.01	0.01	0.006	0.0	0.009	0.003
8	0.0	0.0	0.005	0.005	0.0	0.0	0.001	0.002
9	0.006	0.0	0.003	0.004	-0.001	0.0	0.001	0.001
10	0.0	0.0	0.002	0.002	0.0	0.0	0.0	0.0
11	0.008	0.0	0.001	0.001	0.008	0.0	0.0	0.0

*Systematic b_3 and b_5 are compensated by correctors at each dipole end. The b_3 values in this table indicate the magnitude of the persistent current effect at injection and of the yoke saturation at 8.4 T, the coil geometry being designed for $b_3 = 0$.

Table 3
Estimation of the additional magnetic errors during the ramp of the field for an interstrand contact resistance of 10 μΩ

	Field at x = 1 cm [mT]		Relative field error at injection	
n	normal	skew	b_n	a_n
1	4.8		9.0	0
2	0.03	0.54	0.056	1.0
3	0.24	0.060	0.45	0.11
4	0.018	0.060	0.034	0.11
5	0.091	0.018	0.17	0.034

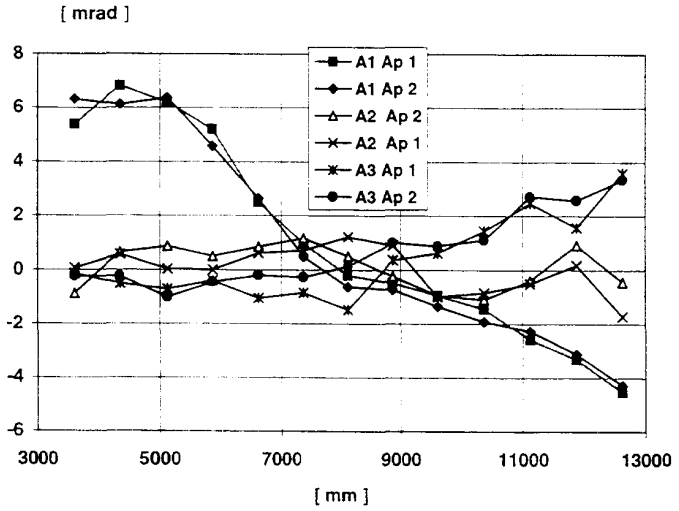

Fig. 17 Field orientation measured in the two apertures of three, 10-m long LHC dipole models (A1, A2, A3)

- Specific heat of materials (NiTi, Cu, etc.) are very low** at 4.2 K (for NbTi, C = ~ 6.5 x 10^{-4} J/g K, for Cu, C = ~ 1 x 10^{-4} J/g K) and is about a factor 10 lower at 2 K.

- A superconductor stays in the s.c. state when temperature, magnetic field and current density are below their critical values.

- The temperature margin, the difference between the conductor working temperature and the critical temperature at the working field and current, is usually very small (1 – 2 K). (E.g. in LHC dipoles ~ 1.2 – 1.4 K.)

- Even extremely small sudden movements of the cable (or even of a strand) or cracking of the insulation generate enough heat to raise local parts of the superconductor above the critical temperature, provoking premature quenching (training).

- It is therefore necessary to limit those sudden movements by a careful design and construction of the force containment structure. Elastic gradual deformations are permitted, to a certain extent.

** ~10^{-4} of the room temperature spec. heat

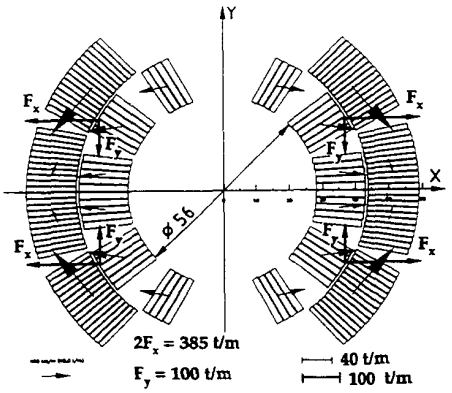

Fig. 18 Transverse electro-magnetic forces in the LHC dipole coils at 9-T field

5.2 "Roman Arch" concept for mechanical stability

Coils are built from different materials: conductors, metallic or insulating spacers, insulations, and glue (epoxy or polyimide resin) to keep everything together, at least during fabrication.

Sometimes the construction is even more loose: one wants to avoid sticking of the insulation to the conductor in order to:

- Let the conductor slide with little friction inside the insulation, to prevent sudden release of heat in case of small movements.

- Let the liquid helium enter into direct contact with the conductor to carry away heat. This is beneficial to stability and essential in case of pulsed magnets or if the magnets have to be operated in helium II (≈2 K), and to remove heat deposited by beam losses (e.g. LHC).

Insulation and glues cannot be relied upon to withstand the high tensile stresses that result from the electromagnetic forces. If nothing is done cracks and micro fissures will develop and the magnet will repetitively quench (training). The solution lies in the application of an adequate pre-compression which will prevent any tensile stress in the coil when e.m. forces are applied. A successful idea was to make the coil behave as a Roman Arch. For $\cos n\vartheta$ winding configurations the external structure applies a radial inward compression which, as in Roman arches, is transformed into azimuthal compression inside the coil which counteracts the formation of tensile stresses that would otherwise appear under the action of the electro-magnetic forces (Fig. 19).

A roman arch can be built from materials of poor or even zero tensile properties (e.g. from dry stones), provided they have a good resistance to compression. For the concept to work the coils should not be supported inside.

This concept was first thought of and applied to the design and construction of the ISR low-β quadrupoles (1974) [23], then adopted in practically all s.c. main magnets for accelerators.

In the example of the ISR quadrupoles (Fig. 20), the pre-compression was applied by means of aluminium-alloy shrinking rings through the yoke quadrants and a set of stainless steel spacers. The main advantages of using an aluminium alloy instead of other materials (e.g. stainless steel) for the shrinking rings were the same as those mentioned in section 5.3 for the collars.

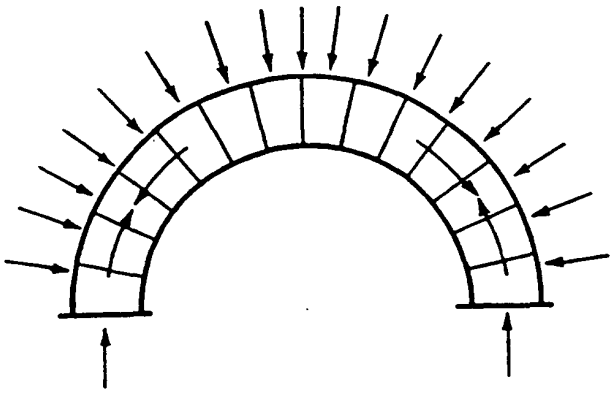

Fig. 19 Roman Arch analogy

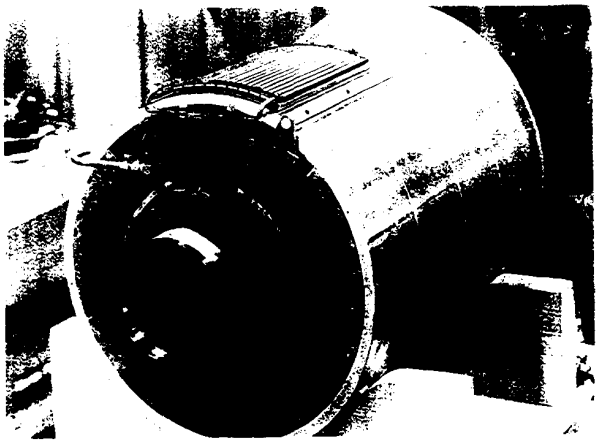

Fig. 20 ISR superconducting quadrupole

5.3 Force-containment structures

The purposes of the force-containment structures are:

- To prevent any sudden movement of the conductors leading to premature quenching and training. For this, the structure must not only be sufficiently strong to hold the e.m. forces without damage, but must also be able to pre-stress the coil in such a way that any tensile stress is prevented at all excitation conditions.

- To limit the elastic deformations of the coils, so that the field quality is maintained at all field levels.

- To guarantee the required structural and dimensional integrity of the magnet.

To achieve this, considerable pre-loads are necessary at operation temperature: e.g. for dipoles operating at 10 T azimuthal average compressive pre-stresses of the order of 80–100 N/mm^2 in the coils are usual.

For magnets working at moderate fields, up to about 5.5 T, coil clamping is in general achieved simply by collars which are adequately compressed when mounted around the coils and locked in position by means of dowels or keys. Different solutions are however adopted concerning the collar material (aluminium alloys, non-magnetic steels, steel-yoke laminations) and their locking system (dowel rods through quasi-circular holes, keys inside grooves).

The main advantage of aluminium alloy collars is that they produce an increase (or at least not a decrease) of the prestress on the coil at cool-down, thanks to their high thermal contraction. In this way the high prestress is applied only when needed and not at room temperature, where creep of insulation or even of copper may occur in the long run. Another advantage is lower cost of material and fabrication. A drawback when compared to stainless or other non-magnetic steels is that more space (wider collars) is required because of lower elastic modulus and tensile/compressive strength. In some cases, however, the coil-to-yoke distance is imposed by the required field quality. In addition, aluminium alloys are more sensitive to stress concentration under fatigue conditions, so that it is not advisable to use grooves and keys to lock them. A problem with present collaring systems is that the coils have to be compressed more than strictly necessary in order to produce the clearances (typically 0.1 mm) which permit the insertion of rods or keys and to compensate for the elongation of the collar "legs" under the reaction of the coils when releasing the press. Concerning the latter, austenitic steels behave better than aluminium alloys owing to their larger elastic modulus (10–20% higher prestress remaining after releasing the press). On the other hand with austenitic-steel collars one is bound

to loose an important fraction (~ 30%) of the prestress during cool-down. This can be accepted in magnets for moderate field levels, but is severely penalizing for high-field magnets in which the prestress that must then be applied at room temperature may exceed the acceptable creep limits (magnets should be able to survive long storage time at room temperature).

It is recognized that to achieve efficient designs for fields above 6 T, it is necessary that the rest of the structure (yoke + other components) contributes to the containment of the forces. So, in the HERA dipoles, which were designed for a lower operation field, above 6 T the collars come in contact in the horizontal plane with the yoke, which acts as a stopper to limit the deformation of the coil/collar assembly [24]. This, however, happens after a non-negligible radial outward elastic expansion (~ 0.1 mm) of the assembly at the median plane.

For the LHC 8 to 10 T dipoles (Fig. 3) a new type of mechanical structure was designed [25] in which aluminium-alloy collars are surrounded by a vertically split yoke (with open gap at room temperature) clamped by a stainless steel shrinking cylinder. The collars are clamped around two coils at room temperature with a moderate pressure to avoid risk of room temperature creep. During the cooling process the shrinkage of the collars increases the pre-compression in the coils, while the yoke halves, which are actuated by the outer shrinking cylinder, move horizontally inwards applying additional compressive forces to the collar-coil assembly in the direction just opposite to the main action of the e.m. forces. The gap between the two parts of the yoke closes at a predetermined lower temperature and when cool-down is completed a compressive force is produced at the mating face between the yoke halves. If this force is equal or larger than the horizontal resultant of the e.m. forces, the gap remains closed in all operating conditions and the split iron behaves as a single stiff solid body. Coil displacement and deformation under the electromagnetic forces are, therefore, greatly reduced, as compared to a simple collar clamping system, with beneficial effects on magnet stability and also on field quality.

In the example of the LHC dipoles at 9 T field the horizontal radial elastic expansion of the coil at the median plane is only about 0.05 mm. In the same conditions the maximum compressive stress in the coil inner layer is 81 N/mm^2, to be compared to 126 N/mm^2 computed for a structure of the same dimensions, but without the compressive prestress on the split-yoke mating faces. The price to be paid for this more efficient, but also more complex structure is that its components have to be produced with tighter dimensional accuracy to ensure that they perfectly fit together.

Axial electro-magnetic forces in high-field magnets produce large stresses and strains in the coil. A quick way to determine globally the axial force is to simply take the derivative of the magnetic stored energy with respect to the axial direction dW/dz. In the LHC 15-m long dipole, at 9.6 T, close to the conductor short sample limit, the stored energy per metre length is 670 kJ, the axial force is then 0.67 MN and the axial tensile stress in the coils would be about 100 MPa and the elastic elongation 12 mm. Magnet ends have, therefore, to be adequately supported by the external structure and a detailed stress analysis has to be done for any end design. Part of the axial force is transferred by friction from the coils to the outer structure, in general the shrinking cylinder, via collars and yoke. The rest is taken by end plates and from them transferred to the strongest longitudinal elements, normally the shrinking cylinder. Sharing between the two parts depends on the construction. Measurements have shown that with the LHC dipole construction type only a fraction of 15–20% of the axial electro-magnetic force is taken by the end plates. Figure 21 is a longitudinal section of the magnet showing the special bolts which carry the force from the coil end pieces to the end plates. These bolts are also used to pre-compress slightly the coil axially at assembly.

Design and stress analysis of the force supporting structures are normally first carried out using the classical mechanical engineering methods and then refined with the aid of modern computer packages which can calculate the e.m. force distribution, the behaviour (stress and strains) of the whole magnet and of each of its components under all operational conditions, and during assembly. Many examples of this procedure can be found in the literature [26, 27], a recent treatment for the LHC dipole is reported in Ref. [28].

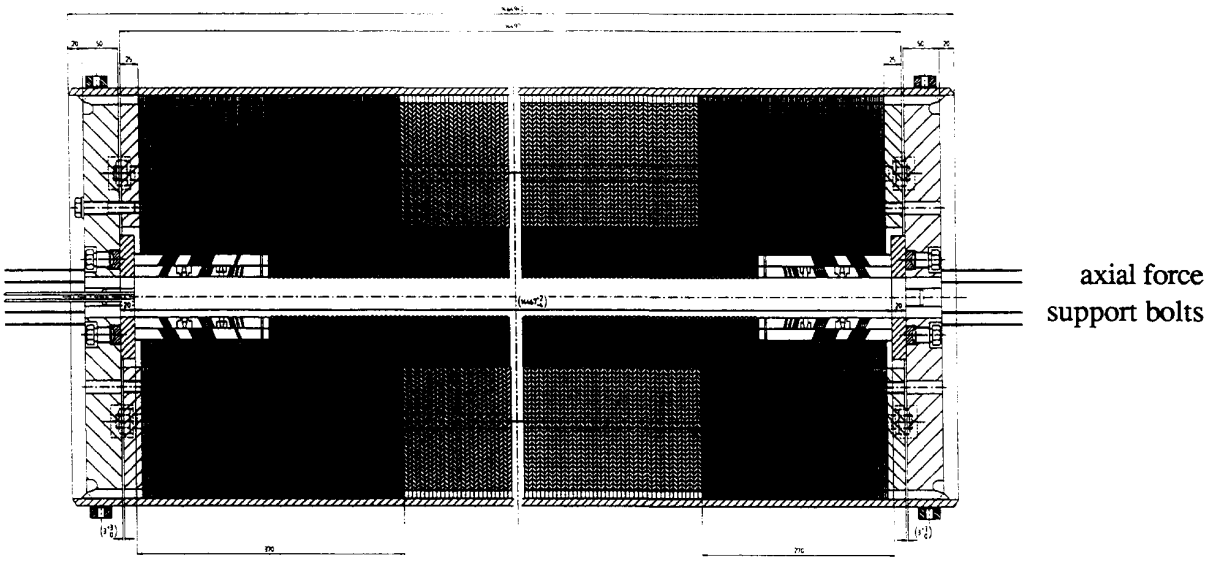

Fig. 21 Longitudinal section of LHC dipole

* * *

REFERENCES

[1] The LHC Study Group, LHC, The large hadron collider accelerator project, CERN/AC/93-03(LHC), 8 Nov. 1993.

[2] M.N. Wilson, Superconducting magnets, Clarendon Press, Oxford 1983.

[3] K.H. Mess, P. Schmüser, Superconducting accelerator magnets, CAS School on Superconductivity in Particle Accelerators, CERN 89-04.

[4] R. Perin, High-field superconducting magnets for particle accelerators, New Techniques for Future Accelerators III, pp. 87-106, Plenum Press, New York, 1990.

[5] M. Linder et al., Construction details and test results from RHIC sextupoles, IEEE Trans. on Magnetics, Vol. 30, No. 4, pp. 1730-1733, July 1994.

[6] P.M. McIntyre, R.M. Scanlan, W. Shen, Ultra-high-field magnets for future hadron collider, Proc. ASC-94, Boston, Oct. 1994.

[7] R.F. Holsinger, Ch. Iselin, CERN POISSON package, CERN computer Library.

[8] R. Perin, S. van der Meer, The program MARE for the computation of two-dimensional static magnetic field, CERN 67-7, March 1967

[9] TOSCA, Vector Fields Ltd, Oxford, U.K.

[10] R.A. Beth, Proc. of 1968 Summer Study on Superconducting Devices, Report BNL 50155, Vol. 3, p. 843, 1968.

[11] R. Perin, Calculation of magnetic field in a cylindrical geometry produced by sector or layer windings, CERN/ISR-MA Internal Note, Nov. 1973.

[12] S. Russenschuck, A computer program for the design of superconducting accelerator magnets, CERN AT/95-39 (MA), LHC Note 354, September 1995.

[13] R. Perin, T. Tortschanoff, R. Wolf, Magnetic design of the superconducting quadrupole magnets for the ISR high-luminosity insertion, CERN/ISR-BOM 179-2, 1979.

[14] T. Tortschanoff, Computation of the integrated field in a s.c. quadrupole magnet with constant perimeter end, Proc. Compumag, 1976.

[15] C. Daum, D. Ter Avest, Three-dimensional computation of magnetic fields and Lorentz forces of an LHC magnet using the method of image currents, Proc. MT-11 Conference, Tsukuba, Japan, 1989.

[16] D. Ter Avest, C. Daum, H.H.J. ten Kate, Magnetic fields and Lorentz forces in an LHC dipole magnet; 3-D analysis using the FEM program TOSCA.

[17] S. Russenschuck and R. Wolf, private communication.

[18] M. A. Green, Residual fields in superconducting magnets, Proc. of Int. Conf. on Magnet Technology, p. 339, 1972.

[19] R. Wolf, Remanent fields in multipoles due to superconductor magnetization, CERN Internal Note ISR-MA, April 1974.

[20] A.P. Verweij, R. Wolf, Field errors due to inter-strand coupling currents in the LHC dipole and quadrupole, CERN Internal Note AT-MA/94-97, March 1994.

[21] T. Ogitsu, Influence of cable eddy currents on the magnetic field of superconducting particle accelerator magnets, SSCL-N-848, January 1994.

[22] V.T. Kovatchev, M.J. Neal, D.W. Capone, W.J. Curr, C. Svenson, Interstrand resistance of SSC magnets, Cryogenics 1994, Vol. 34, No. 10.

[23] R. Perin, Mechanical stability of superconducting quadrupole coils, Proc. 5th Int. Conf. on Magnet Technology, pp. 551-556, Roma, 1975.

[24] H. Kaiser, Design of superconducting dipole for HERA, 13th Int. Conf. on High Energy Accelerators, Novosibirsk, 1986, and DESY-HERA 1986-14.

[25] R. Perin, Preliminary views on 8 tesla dipole magnet for the Large Hadron Collider, CERN LHC Note 32, and CERN-TIS-MC/85-2.

[26] D. Leroy, R. Perin, G. de Rijk, W. Thomi, Design of a high-field twin-aperture superconducting dipole model, IEEE Trans. on Magnetics, Vol. 24, pp. 1373-1376, March 1988.

[27] D. Leroy, R. Perin, D. Perini, A. Yamamoto, Structural analysis of the LHC 10 T twin-aperture dipole, Proc. XI Int. Conf. on Magnet Technology, pp. 159-164, Tsukuba, Japan, 1989.

[28] R. Perin, D. Perini, J. Salminen, J. Soini, Finite element structural analysis of LHC bending magnet, Proc. MT14, Tampere, 12-15 June 1995.